Journal of Coastal Research	27	6A	44–51	West Palm Beach, Florida	November 2011

GIS Modelling of Intertidal Wetland Exposure Characteristics

Nathan Crowell[†], Timothy Webster[†], and Nelson J. O'Driscoll[‡]

[†]Applied Geomatics Research Group
Nova Scotia Community College
Middleton, Nova Scotia,
B0S 1P0, Canada
Nathan.Crowell@nscc.ca

[‡]Department of Earth and Environmental Science
Acadia University
Room LL33 K.C. Irving Environmental Science Centre
Wolfville, Nova Scotia, B4P 2R6, Canada

www.cerf-jcr.org

www.JCRonline.org

ABSTRACT

CROWELL, N.; WEBSTER, T., and O'Driscoll, N.J., 2011. GIS modelling of intertidal wetland exposure characteristics. *Journal of Coastal Research,* 27(6A), 44–51. West Palm Beach (Florida), ISSN 0749-0208.

Exposure to solar radiation and tidal inundation are important factors for a wide variety of chemical and ecological processes in coastal ecosystems. Accurate quantification of these factors is often difficult on a local scale. To address this research gap, a remote-sensing approach was developed to model inundation and radiation characteristics within an intertidal zone located in the Minas Basin (Bay of Fundy, Nova Scotia, Canada). A light detection and ranging (LIDAR)–derived elevation model was subjected to tidal modelling based on hourly sea level predictions and solar modelling based on sunrise and sunset times for 2009. Model results indicated an intertidal zone of 145.8 km^2 with an elevation between −6.9 m and 6.8 m. The intertidal zone was determined to contain three unique wetland classes: (1) 4.4 km^2 of high salt marsh, dominated by *Spartina patens*; (2) 5.0 km^2 of low salt marsh, dominated by *Spartina alterniflora*; and (3) 63.1 km^2 of nonvegetated marine flat (73.3 km^2 unclassified intertidal). Detailed exposure characteristics were calculated for each of the classes within the intertidal zone at 10-cm vertical intervals. Exposure calculations for 2009 showed that an average of 4.2 km^2 of salt marsh were exposed to solar radiation and 8.4 km^2 were exposed to the atmosphere each hour. Similarly, 11.7 km^2 of marine flat were exposed to solar radiation and 22.9 km^2 were exposed to the atmosphere each hour. The developed remote-sensing techniques successfully established intertidal zones, uniquely identified wetland classes, and modelled inundation and solar exposure characteristics within the study area.

ADDITIONAL INDEX WORDS: *LIDAR, inundation, solar radiation, coast, salt marsh, marine flat.*

INTRODUCTION

Solar radiation provides primary producers with the energy needed for photosynthesis and is a critical factor in the productivity of an ecosystem (Begon, Townsend, and Harper, 2006). The consumption of abundant primary producers facilitates the passing of stored energy between trophic levels throughout the food web. Ecosystems which exhibit high primary production often support a greater number of trophic levels and therefore result in high measures of biodiversity (Pimm, Lawton, and Cohen, 1991). Biodiversity is thought to reflect both the stability and predictability of an ecosystem and is considered one of the most critically important measures in ecology (McGrady-Steed, Harris, and Morin, 1997). Solar radiation is also critical in many photoreactions which control the fate of contaminants in wetlands. For example, mercury is converted to volatile dissolved gaseous mercury, which is highly volatile and degasses from freshwaters and sediments in intertidal ecosystems (Canário and Vale, 2004; O'Driscoll *et al.*, 2008). By quantifying the studied ecosystem's exposure to solar radiation, it is possible to improve our understanding of the dependent processes within the area of study.

In addition to solar radiation exposure, tidal inundation patterns are a determining factor in sediment chemical characteristics, plant species composition, and contaminant fate. Increased periods of inundation result in lower levels of available oxygen in sediments as depth increases. These heterogeneous, anaerobic conditions can influence the distribution of wetland plant species (DeLaune, Pezeshki, and Patrick, 1987) and may enhance the formation of toxic methylmercury (MeHg) (Canário *et al.*, 2007). Prolonged flooding also leads to the buildup of chemical compounds such as sulfide and similar toxins which are deleterious to plant systems by preventing nitrogen uptake and root development (DeLaune, Smith, and Patrick, 1983). In intertidal zones, the viability of salt-tolerant plant species such as *Spartina alterniflora* and *Spartina patens* is also highly dependent on their ability to efficiently overcome the anaerobic environment and transport O_2 to their root systems (Gleason and Zieman, 1980). *Spartina alterniflora* is able to effectively transport O_2 during longer periods of inundation and can therefore persist at lower elevations than *S. patens* within intertidal zones. Millard *et al.* (2006) have demonstrated that accurate inundation models can predict viable locations for wetland flora species to

DOI: 10.2112/JCOASTRES-D-10-00187.1 received 6 December 2010; accepted in revision 13 February 2011.
Published Pre-print online 8 June 2011.

grow and may be of particular interest to coastal wetland restoration initiatives.

Accurate modelling of solar radiation availability, food chain dynamics, oxygen availability, and chemical speciation are difficult due to local differences in topography that create variances in inundation and solar-exposure regimes. Radiation is often recorded only at specific sampling sites and is not reflective of coastal dynamics at the sediment level. This practice limits the external application of the data to areas of heterogeneous exposure, which are often unrepresentative of the ecological zones in which sampling occurs. This fact is especially true for highly dynamic intertidal zones in which solar exposure is often dictated by tidal level. Furthermore, inundation patterns for specific study areas are often derived from coarse-resolution models of topography, which have limited use in predicting the true location of highly sensitive chemical processes or species distribution.

Geographic information systems (GISs) can help solve these problems by incorporating high-resolution digital elevation models (DEMs) and advanced predictive modelling, allowing researchers to model complex environmental interactions within geographically accurate systems. The development of properly modelled exposure characteristics within a spatial context could extend localized findings throughout the ecological zone of interest.

Light detection and ranging (LIDAR)–derived DEMs have proven to be a highly accurate medium for modelling terrain (Krabill *et al.*, 1995; Shrestha *et al.*, 1999). High-resolution terrain modelling has been applied to scientific studies in various fields such as geomorphology for the investigation of fault monitoring (Chan *et al.*, 2007), coastal water and mudflat modelling (Brzank *et al.*, 2008), tidal channel modelling (Mason, Scott, and Wang, 2006), estuary floodplain modelling (French, 2003), and coastal flood-risk mapping from sea level rise and storm surge events (Webster, Mosher, and Pearson, 2008; Webster *et al.*, 2006). It is expected that a LIDAR-derived DEM would serve as a suitable base to model coastal and intertidal environments.

This study was developed to address two principle hypotheses: (1) solar radiation and atmospheric exposure can be successfully modelled within a GIS environment based on a LIDAR-derived DEM and existing wetland mapping information, and (2) once modelled, the information would provide exposure characteristics for each 4-m^2 cell within the study area.

METHODS

Study Area

Intertidal and terrestrial components of the Southern Bight portion of the Minas Basin, located within the eastern segment of the Bay of Fundy, between Kings County and Hants County, Nova Scotia, Canada, served as the area of analysis (Figure 1).

The Bay of Fundy is characterized by a semidiurnal tidal cycle which generates two flood tides and two ebb tides per day. The average macrotidal range is 13 m, though storm surges may push the range over 16 m (Percy, 2001). The Southern Bight was added to the Ramsar List of Wetlands of International Importance in November 1987. It is composed primarily of extensive intertidal marine flat, intertidal vegetated salt marsh, estuarine waters, and marine waters. The marine flats host a plethora of invertebrate organisms (Wells *et al.*, 2004) which sustain the largest number of mixed-species shoreline birds in all of North America during fall migrations (Ginn and Hamilton, 2009).

Digital Elevation Model Production

Digital elevation data were obtained using an airborne LIDAR system. LIDAR is a remote-sensing system which couples laser altimetry with GPS and inertial-measurement information to collect high-precision point elevation observations at very high densities. Information on formulas used to extract point elevation data may be found in Baltsavias (1999). Elevation data were acquired by the Applied Geomatics Research Group (AGRG; Middleton, Nova Scotia, Canada) in 2003 using a Mark I LIDAR system (Terra Remote Sensing Inc., Sidney, British Columbia, Canada) for the western extent of the study area, and in 2007 utilizing an ALTM 3100 LIDAR system for the eastern extent. The AGRG team surveyed the study area at low tide, insuring maximum intertidal coverage. Point elevation data were classified into ground hits, using the ground/nonground separation algorithm within the MicroStation V8 2004 TerraScan software interface. The ground LIDAR points were subsequently used to form a triangular irregular network (TIN). The TIN surface was then used to construct a high-resolution bare-earth DEM raster (4-m^2 cell size) based on a linear interpolation method. Accuracy assessment of the DEM was performed by AGRG using real time kinematic–derived ground control points (with a Leica 530), in accordance with standardized procedures (Webster, 2005; Webster and Dias, 2006). Vertical specifications of 30 cm in the 2003 data set and 15 cm in the 2007 data set were confirmed before modelling was executed.

Tidal Inundation Model

Tidal modelling was executed using a predictive approach. Tidal predictions were obtained for 2009 at 1-hour intervals from Flater and Pentcheff (2009) to serve as a basis for analysis ($n = 8760$). Tidal water elevations were converted from a local chart datum (Hantsport, Nova Scotia) to orthometric heights above the Canadian Geodetic Vertical Datum 1928 using a constant offset of −7.23 m. This conversion ensured that water elevation predictions were in a common frame of reference with DEM elevations. The minimum and maximum tidal elevations were predicted to be −6.89 m and 6.76 m, respectively. The difference between these boundaries defined the inundation elevation range required for modelling (13.65 m). Modelling occurred within the ArcGIS 9.3 interface using a Visual Basic 6 script developed to identify high-risk areas for flood damage from storm surge events and sea level rise (Webster and Stiff, 2008). The script uses cell elevations within the LIDAR-derived DEM raster to determine hydrologic connectivity between adjacent cells in order to mimic static flood levels without accounting for preservation of momentum or rate of flow. In

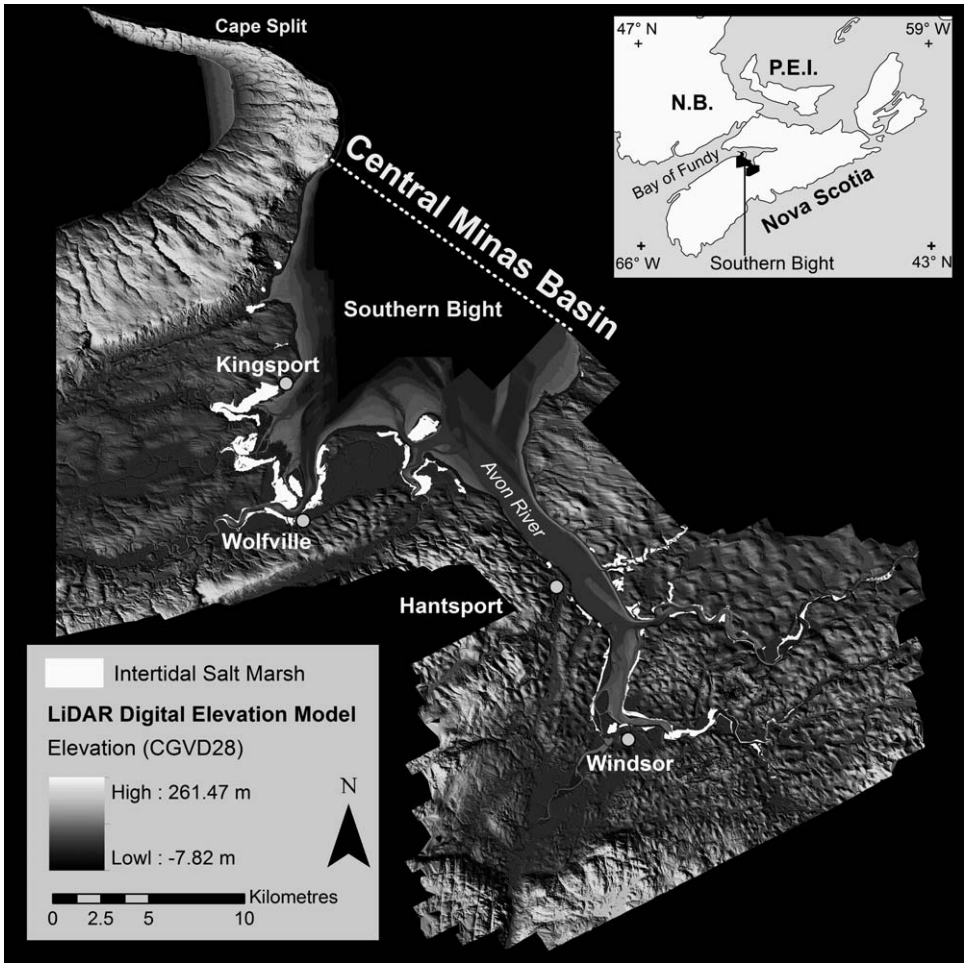

Figure 1. Overview of the study area, located in the southern Minas Basin, Nova Scotia, Canada. The area is denoted by a shaded relief map based on a LIDAR-derived DEM. Intertidal salt marsh locations were delineated based on model results.

this way, water levels were modelled and delineated in a realistic manner within the DEM at 0.1-m elevation intervals over the full 13.65-m tidal range.

Modelling produced 137 delineated tidal snapshots which mimicked water position over the intertidal terrain. These observations were linked back to the temporal tidal predictions in order to attribute spatial characteristics to each of the observations (n = 8760). As such, it was possible to quickly assess the area of exposure and submergence for each tidal prediction to the nearest 0.1-m elevation. Once these were linked, it was also possible to extract detailed spatial information regarding known features, such as salt marshes and marine flats, based on tidal predictions.

Solar Exposure Model

Sunrise and sunset times were obtained for 2009 (Astronomical Applications Department, 2009) in order to classify areas corresponding to each tidal prediction as either exposed or shaded. It is important to note that no shading calculations were performed using elevation models, and that intertidal areas were classified as exposed to solar radiation if (1) there was daylight during the time of the tidal prediction and (2) the area was greater in elevation than the predicted tidal elevation. This logic was employed for each individual observation to yield annual solar-exposure characteristics as a percent time exposed (n = 8760). The results were linked to the 137 tidal delineations in order to visualize and further analyze the findings within the intertidal zone.

Coastal Wetland Zones

Salt marshes are chemically and ecologically very different than intertidal marine flats due to the presence of salt-tolerant vegetation such as *S. alterniflora* and *S. patens*. To maintain this variability throughout the analysis, three distinct classes were developed to account for (1) low salt marsh areas, predominantly vegetated by *S. alterniflora*; (2) high salt marsh areas, in which *S. patens* was the dominant vegetation; and (3) marine flats, which were characterized as nonvegetated areas with minimal relief. The three classes were separated from general intertidal analysis and were individually analyzed over

the 137 tidal delineations. Spatial extents for each of the three classes were obtained from the Nova Scotia Wetlands and Coastal Habitats Inventory produced by the Nova Scotia Department of Natural Resources (DNR), Renewable Resources Branch, Wildlife Division, in 2000. These data were implemented in the GIS to delineate low salt marsh, high salt marsh, and marine flat locations within the study area. Once established, intertidal analysis was executed on each of the layers using a script developed within the Python 2.5 interface for ArcGIS 9.3. The script was designed to cycle through all tidal model delineations ($n = 137$) and determine spatial overlap between each layer of interest and tidal water level. If overlap occurred, the tidal level was recorded and the zone of intersection was extracted and delineated as submerged. Because exposure to atmosphere and solar radiation is dependent on submergence, the annual atmospheric and solar-exposure characteristics attributed to each water level could also be applied to the newly established areas of submergence. Analysis was executed in this fashion from the lowest modelled elevation (−6.9 m) to the highest (6.8 m). When complete, the script provided atmospheric and solar-exposure characteristics for each of the examined layers at 0.1-m elevation increments within the intertidal zone.

Calculations

Although spatially based, the majority of calculations were executed outside of the GIS in the Microsoft Excel 2010 interface. Atmospheric exposure occurred when an area was above any modelled tidal elevation. The portion of time this area was exposed to the atmosphere could be determined by calculating the total number of tidal predictions at elevations below the elevation of interest and dividing by the total number of predictions. Equation (1) was used to calculate the annual exposure characteristics.

$$T_{\mathrm{Atm}Z} = \left[\frac{\sum (Tide_{<Z})}{Tide_{\mathrm{Obs}}}\right] \times 100 \qquad (1)$$

where $T_{\mathrm{Atm}Z}$ = the percentage of time exposed to the atmosphere at elevation Z, Z = the predicted tidal elevation of the observation being examined (in m), $Tide_{<Z}$ = the number of tidal observations less than the examined observation, and $Tide_{\mathrm{Obs}}$ = the total number of tidal observations.

Similarly, solar exposure was defined as occuring only when areas were at an elevation above a given tidal prediction and were attributed a sun-exposed value. The portion of time each model height spent exposed to solar radiation could be determined by taking the sum of the number of sun observations at elevations less than or equal to the tidal prediction, minus the number of observations at the tidal prediction. Equation (2) was used to calculate solar exposure.

$$T_{\mathrm{Sol}Z} = \left[\frac{\sum (Sol_{<Z} - Sol_{Z})}{Tide_{\mathrm{Obs}}}\right] \times 100 \qquad (2)$$

where $T_{\mathrm{Sol}Z}$ = the percentage of time exposed to solar radiation at elevation Z, Z = the predicted tidal elevation of the observation being examined (in m), $Sol_{<Z}$ = the number of solar observations at elevations less than the examined observation, Sol_{Z} = the number of solar observations at elevations equal to the examined observation, and $Tide_{\mathrm{Obs}}$ = the total number of tidal observations.

The calculations were performed for each of the 8760 tidal predictions rounded to the nearest 0.1-m elevation. Results were linked to the already established 0.1-m tidal elevation increments for further GIS spatial analysis. A database was developed which contained annual exposure characteristics linked to all intertidal, salt marsh, and marine flat zones. The results were also used in temporal analysis and were broken into daily and monthly averages.

RESULTS

General Intertidal Characteristics

The LIDAR-surveyed area spanned 1004.2 km² (288.3-m elevation). The intertidal zone was predicted to be between −6.89 m and 6.76 m (a 13.65-m range) vertically and cover 145.8 km² from January 1, 2009, to December 31, 2009. Monthly averages of tidal elevation showed little variation over the 2009 cycle (mean = 0.27 m; SD = 0.06 m). Annual atmospheric exposure was found to be strongly correlated to intertidal elevation (r = 0.99; $p < 0.01$), though oscillations were observed due to the cyclic nature of tidal elevations (Figure 2). The proportion of daylight hours for 2009 was found to be more variable (mean = 0.51; SD = 0.11); it was highest during the month of June (0.67) and lowest during the month of December (0.35), as was expected given the latitude of the study area. The exposure to sunlight was also found to be nearly perfectly correlated to intertidal elevation (r = 0.99; $p < 0.01$), peaking at 51.1% annual exposure to sunlight at a 5.9-m elevation (Figure 2).

Coastal Wetland Characteristics

Wetland classes were evaluated separately and are summarized in Table 1. Marine flats covered 73.7 km² of the study area, of which 63.1 km² (86%) were found within the intertidal zone. Vegetated wetlands were divided into high salt marsh and low salt marsh classes. High salt marshes covered 13.9 km² of the study area, with 4.4 km² (32%) of this area found within the intertidal zone. Low salt marsh covered 5.7 km² of the study area, with 5.0 km² (88%) of this area located within the intertidal zone. Vegetated wetland coverage was found to be concentrated above the average annual tidal elevation (0.27 m), as seen in Figure 2. The average daily atmospheric exposure exhibited little variability for each of the classes, while daily solar exposure was more variable due to seasonal trends (Table 2). Monthly statistics showed that intertidal areas were exposed to the maximum solar radiation during the month of June for each of the wetland classes, marine flat (15.6 km²), high salt marsh (2.8 km²), and low salt marsh (2.8 km²). Minimum exposure to solar radiation occurred during the month of December for each of the wetland classes, marine flat (7.2 km²), high salt marsh (1.5 km²), and low salt marsh (1.4 km²) (Figure 3).

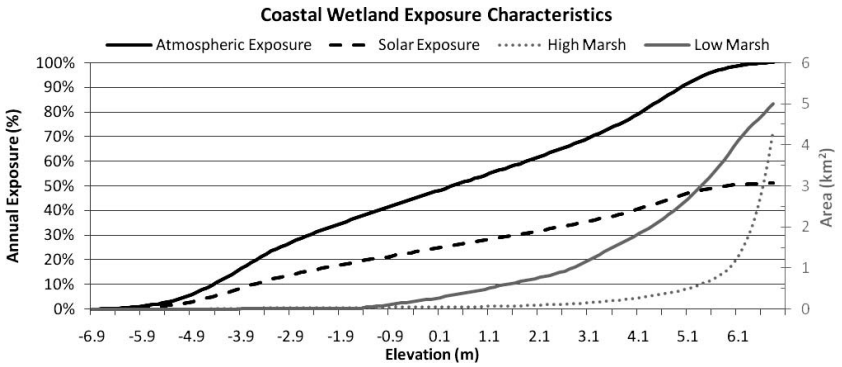

Figure 2. Modelled coastal wetland exposure characteristics based on sun position and tidal elevation predictions for 2009, showing the percentage of time per annum coastal wetlands spent exposed to the atmosphere (solid back) and solar radiation (dashed black) for corresponding areas of high salt marsh (dotted grey) and low salt marsh (solid grey) plotted against wetland elevations derived from LIDAR DEM data.

GIS Analysis

Tidal modelling was found to produce realistic water delineations based on predicted tidal elevations. The model produced 137 delineations between elevations of −6.9 m and 6.8 m at 0.1-m increments. The extraction of submerged areas using a developed Python 2.5 script allowed for subsequent integration of salt marsh and marine flat exposure data in the GIS (Figure 4).

DISCUSSION

Salt Marsh Analysis

The low percentage of high salt marsh areas, dominated by *S. patens*, within the intertidal zone (32%) can be explained by the nature of this species and tidal predictions. *Spartina patens* is a salt-tolerant grass which cannot survive regular inundation in salt water but can thrive in fringe areas which are only inundated during irregularly high tides. These irregular tides are not captured by the tidal predictions used in this study, which only account for astronomical tidal constituents. On the contrary, *S. alterniflora* is able to survive regular inundation in salt water and is found more frequently within the astronomically defined intertidal zone (88%). Atmospheric modelling of the intertidal zone has provided a quantified depiction of O_2 availability and rate of submergence within the study area. These data are particularly useful for studies that examine variables which are sensitive to these factors, such as wetland restoration initiatives, species composition predictions, and biodiversity predictions.

Table 1. *Summary of intertidal wetland class characteristics.*

	Marine Flat	High Salt Marsh	Low Salt Marsh
Total area (km²)	73.7	13.9	5.7
Intertidal area (km²)	63.1	4.4	5.0
Minimum elevation (m)	−6.9	−5.5	−5.5
Maximum elevation (m)	6.8	6.8	6.8

Areas of salt marsh were found to extend to unexpectedly low elevations (−5.5 m). On further analysis, it was found that delineations performed by the Nova Scotia Department of Natural Resources were limited when compared to real-world salt marsh locations observed in high-resolution (1 : 10,000 scale) aerial photography acquired by Service Nova Scotia in July of 2002. The discrepancies between observed salt marsh locations and DNR delineations were primarily due to substantial differences between the date of delineation by DNR and LIDAR data collection. Findings from Percy (2008) support this claim, as large zones of newly established salt marsh in close proximity to the town of Windsor were absent from the DNR data set. The temporal discrepancy most likely resulted in erroneously low salt marsh elevations by not accounting for short-term morphological changes within DNR-delineated salt marsh areas. Specifically, morphological changes such as channeling could account for a large portion of the unexpectedly low elevations. The discrepancy also accounts for the results presented in Table 1 which exhibit realistic proportions of intertidal area for both high and low salt marsh classes, despite having identical minimum and maximum elevations. Observed elevation errors led to overestimation of the intertidal areas of high salt marsh locations and underestimation of the intertidal areas of low salt marsh locations. This skewing, along with the nature of exposure at higher elevations, resulted in identical average daily exposure characteristics between high and low salt marsh classes (Table 2).

Table 2. *Average daily intertidal exposure characteristics for each of the three wetland classes.*

	Marine Flat	High Marsh	Low Marsh
Atmospheric exposure (km²)			
Average	22.9	4.2	4.2
SD	1.23	0.07	0.18
Solar exposure (km²)			
Average	11.74	2.1	2.1
SD	3.34	0.46	0.50

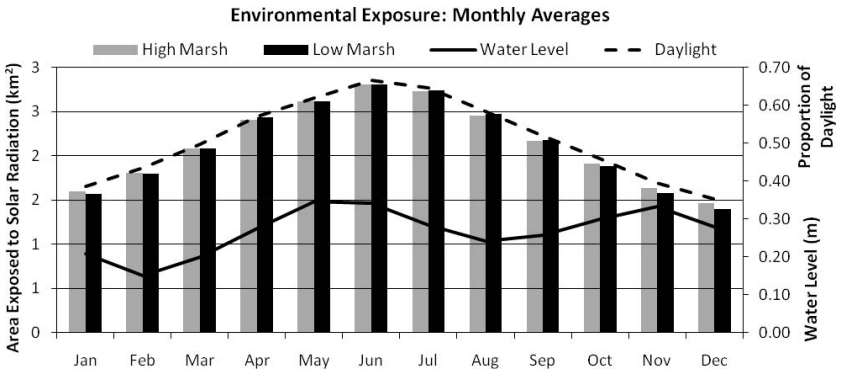

Figure 3. Predicted monthly averages (2009) for areas of high marsh (light grey bars) and low marsh (dark grey bars) exposed to solar radiation. The proportion of daylight hours (dashed black line) is based on sunrise and sunset times, and water level (solid black line) is based on hourly tidal predictions (2009). The areas of exposed salt marsh classes were calculated using the developed inundation model.

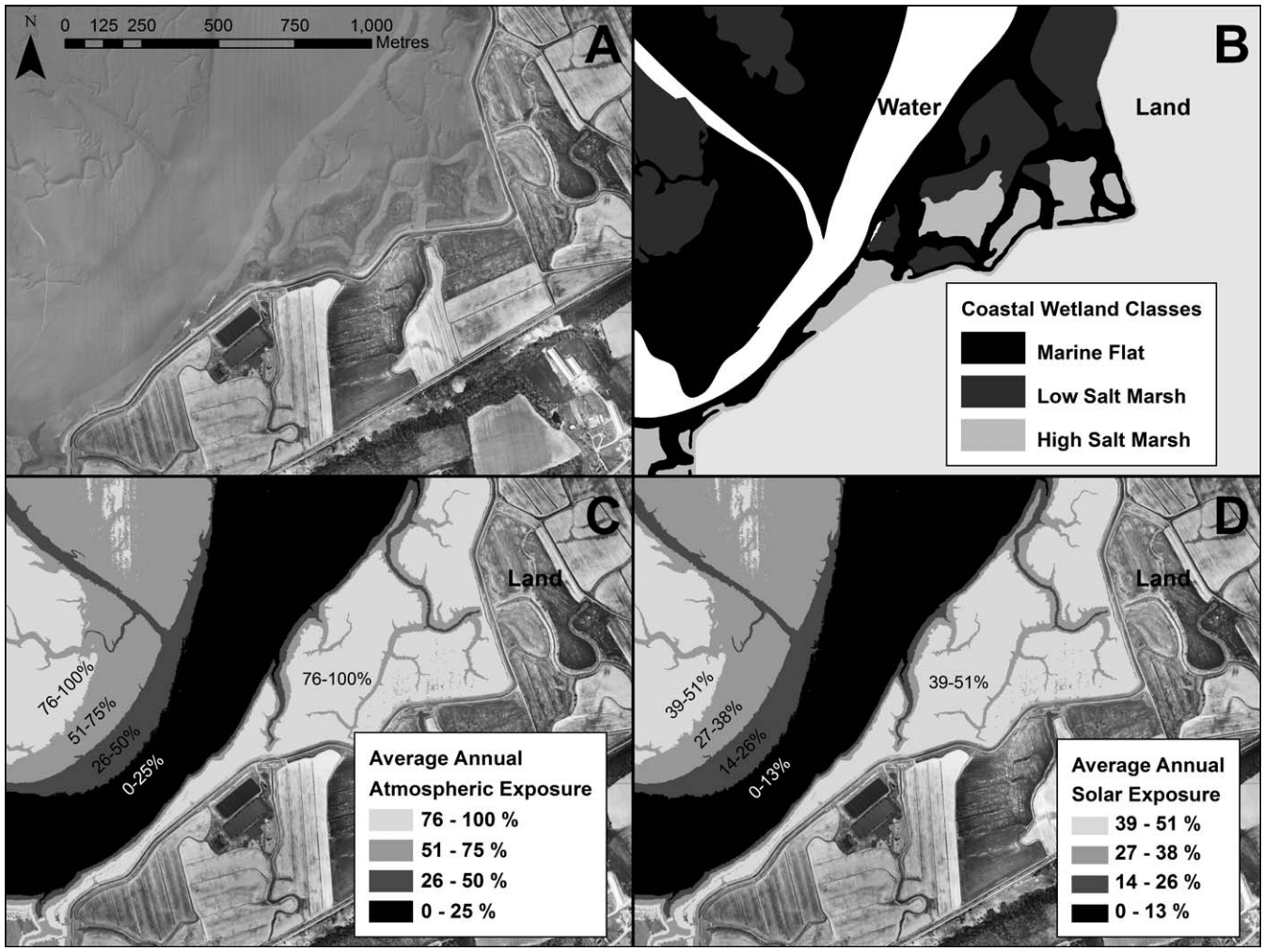

Figure 4. (A) Orthorectified imagery for a region of intertidal wetland separated from agricultural land by a protective dyke to the NE of Wolfville, Nova Scotia, Canada taken in 2006. The model results were overlaid to depict (B) delineated wetland classes based on dominant vegetation, (C) atmospheric exposure characteristics of the intertidal zone based on hydrographic modelling which examined topography and hourly tidal predictions for 2009, and (D) solar exposure characteristics of the intertidal zone based on hydrographic modelling and astronomical predictions.

Despite temporally based inaccuracies discovered within the DNR data set, the data were delineated at a high resolution and contained an attribute table which allowed for wetland classification based on dominant vegetation. The layer was determined to be suitable for analysis as a means for addressing the principal hypotheses of the study.

Solar Characteristics

Simple observational categories such as solar-exposed or shaded were implemented to measure the period of time intertidal areas spent exposed to the sun during 2009. The GIS analysis successfully attributed precise exposure times to all 4-m² cells within the intertidal zone. Though this method was found to be useful, it is possible to implement more complex models for solar exposure. Further study could incorporate a more complex model which would account for true radiation values expressed in the appropriate units. Similarly, terrain shadowing and sun angle characteristics could be accounted for, although these are not expected to be significant given the observed intertidal topography.

Further Implications

It should be noted that, although this analysis focused on salt marsh and marine flat coverage, the developed tool set may be used to analyze any spatially relevant data without change to the underlying methodology. For example, if concentrations of a photochemically reactive chemical or contaminant such as MeHg were quantified in an area, the area could be delineated and its solar-exposure characteristics quantified to examine residence time of the toxic compound. Once established, concentrations of MeHg could be extended to homogeneous zones within the study area. The result would be a spatially accurate quantification of contaminant distribution. Similarly, if redox potentials were known for a particular inundation regime, areas could be delineated by the model in order to quantify their contributory areas based on atmospheric exposure. In this way, model data have the potential to extend the findings of studies such as O'Driscoll, Lean, and Renez (2005) and O'Driscoll *et al.* (2008) which meticulously measure the formation and volatilization of toxic compounds over varying environmental factors. The relationship between the changing compound and environmental exposure can be maintained within the model in order to accurately depict volume of change based on exposure characteristics throughout the area of study.

CONCLUSIONS

Tidal elevation and solar exposure are dynamic variables which directly influence a wide variety of ecological and geochemical characteristics. Based on the developed model, it was possible to quantify the relationship between these variables and a highly accurate terrain model through the use of GIS. The model developed in this study could be used by multiple disciplines to quantify ecological and geochemical conditions in a heterogeneous environment in order to further extrapolate localized findings to larger zones within the study area which exhibit the same coverage and exposure characteristics.

ACKNOWLEDGMENTS

Funding for this research was provided in a grant from the National Sciences and Engineering Research Council of Canada (NSERC) and the Canada Research Chairs Program to Dr. Nelson O'Driscoll. Funding for LiDAR was provided by the Canada Foundation for Innovation and collaboration with Dr. Danika van Proosdij of Saint Mary's University.

LITERATURE CITED

Astronomical Applications Department. Sun or moon rise/set table for one year. http://aa.usno.navy.mil/data/docs/RS_OneYear.php (accessed January 21, 2009).

Baltsavias, E.P., 1999. Airborne laser scanning: basic relations and formulas. *Journal of Photogrammetry and Remote Sensing*, 54, 199–214.

Begon, M.; Townsend, C.R., and Harper, J.L., 2006. *Ecology: From Individuals to Ecosystems*. Malden, Massachusetts: Blackwell Publishing, 738p.

Brzank, A.; Heipke, C.; Goepfert, J., and Soergel, U., 2008. Aspects of generating precise digital terrain models in the Wadden Sea from lidar–water classification and structure line extraction. *Journal of Photogrammetry and Remote Sensing*, 63, 510–528.

Canário, J. and Vale, C., 2004. Rapid release of mercury from intertidal sediments exposed to solar radiation: a field experiment. *Environmental Science and Technology*, 38, 3901–3907.

Canário, J.; Caetano, M.; Vale, C., and Cesário, R., 2007. Evidence for elevated production of methylmercury in salt marshes. *Environmental Science and Technology*, 41, 7376–7382.

Chan, Y.C.; Chen, Y.G.; Shih, T.Y., and Huang, C., 2007. Characterizing the Hsincheng active fault in northern Taiwan using airborne LiDAR data: detailed geomorphic features and their structural implications. *Journal of Asian Earth Sciences*, 31, 303–316.

DeLaune, R.D.; Pezeshki, S.R., and Patrick, W.H., Jr., 1987. Response of coastal plants to increase in submergence and salinity. *Journal of Coastal Research*, 3, 536–546.

DeLaune, R.D.; Smith, C.J., and Patrick, W.H., Jr., 1983. Relationship of marsh elevation, redox potential, and sulfide to *Spartina alterniflora* productivity. *Soil Science Society of America Journal*, 47, 930–935.

Flater, D. and Pentcheff, D. Tide/current predictor. http://tbone.biol.sc.edu/tide/tideshow.cgi?site=Hantsport%2C+Nova+Scotia (accessed January 24, 2009).

French, J.R., 2003. Airborne LIDAR in support of geomorphological and hydraulic modelling. *Earth Surface Processes and Landforms*, 28, 321–335.

Ginn, M.G. and Hamilton, D.J., 2009. Food habits and foraging behaviour of semipalmated sandpipers (*Calidris pusilla*) during migratory stopover in the upper Bay of Fundy, New Brunswick. *In: Proceedings of the 8th Bay of Fundy Science Workshop* (Wolfville, Nova Scotia), 177p.

Gleason, M.L. and Zieman, J.C., 1980. Influence of tidal inundation on internal oxygen supply of *Spartina alterniflora* and *Spartina patens*. *Estuarine, Coastal and Shelf Science*, 13, 47–57.

Krabill, W.B.; Thomas, R.H.; Martin, C.F.; Swift, R.N., and Frederick, E.B., 1995. Accuracy of airborne laser altimetry over the Greenland ice sheet. *International Journal of Remote Sensing*, 16, 1211–1222.

Mason, D.C.; Scott, T.R., and Wang, H.J., 2006. Extraction of tidal channel networks from airborne scanning laser altimetry. *Journal of Photogrammetry and Remote Sensing*, 61, 67–83.

McGrady-Steed, J.; Harris, P.M., and Morin, P.J., 1997. Biodiversity regulates ecosystem predictability. *Nature*, 390, 162–165.

Millard, K.; Webster, T.; Stewart, H.; Colville, D., and Redden, A., 2006. Salt marsh species zonation in the Minas and Cumberland basins: using LIDAR to examine salt marsh vegetation. *In:*

Proceedings of the 7th Bay of Fundy Science Workshop (St. Andrews, New Brunswick), pp. 122–124.

O'Driscoll, N.J.; Lean, D.R., and Renez, A.N., 2005. Review of factors affecting mercury fate in Kejimkujik Park, Nova Scotia. *In:* O'Driscoll, N.J.; Renez, A.N., and Lean, D.R. (eds.), *Mercury Cycling in a Wetland Dominated Ecosystem: A Multidisciplinary Study*. Pensacola, Florida: Society of Environmental Toxicology and Chemistry, pp. 5–12.

O'Driscoll, N.J.; Poissant, L.; Canário, J., and Lean, D., 2008. Dissolved gaseous mercury concentrations and mercury volatilization in a frozen freshwater fluvial lake. *Environmental Science and Technology*, 42, 5125–5130.

Percy, J.A., 2001. Fundy's Minas Basin: Multiplying the Pluses of Minas. Bay of Fundy Ecosystem Partnership Fundy Issues Fact Sheet 19, http://www.bofep.org/minas1.htm.

Percy, J.A., 2008. The "Cause" in Causeway: Crossing the Avon River at Windsor. Bay of Fundy Ecosystem Partnership Fundy Issues Fact Sheet 28, pp. 1–12.

Pimm, S.L.; Lawton, J.H., and Cohen, J.E., 1991. Food web patterns and their consequences. *Nature*, 350, 669–674.

Shrestha, R.L.; Carter, W.E.; Lee, M.; Finer, P., and Sartori, M., 1999. Airborne laser swath mapping: accuracy assessment for surveying and mapping applications. *Surveying and Land Information Systems*, 59(2), 83–94.

Webster, T.L., 2005. LIDAR validation using GIS: a case study comparison between two LIDAR collection methods. *Geocarto International*, 20, 11–19.

Webster, T.L. and Dias, G., 2006. An automated GIS procedure for comparing GPS and proximal LIDAR elevations. *Computers and Geosciences*, 32, 713–726.

Webster, T.L.; Forbes, D.L.; MacKinnon, E., and Roberts, D., 2006. Floodrisk mapping for storm-surge events and sea-level rise in southeast New Brunswick. *Canadian Journal of Remote Sensing*, 32, 194–211.

Webster, T.L.; Mosher, R., and Pearson, M., 2008. Water Modeler: A component of a coastal zone decision support system to generate flood-risk maps from storm surge events and sea-level rise. *Geomatica*, 62, 393–406.

Webster, T. and Stiff, D., 2008. The prediction and mapping of coastal flood risk associated with storm surge events and long-term sea level changes. *In:* Brebbia, C.A. and Beriatos, E. (eds.), *Risk Analysis VI: Simulations and Hazard Mitigation*. Southampton, United Kingdom: WIT Press, pp. 129–139.

Wells, P.G.; Daborn, G.R.; Percy, J.A.; Harvey, J., and Rolston, S.J., 2004. Health of the Bay of Fundy: assessing key issues. *In: Proceedings of the 5th Bay of Fundy Science Workshop and Coastal Forum* (Wolfville, Nova Scotia), pp. 327–333.